Temporal response of an atom to a stochastic field: Resonant enhancement of population fluctuations at the Rabi frequency

J. C. Camparo, J. G. Coffer, and R. P. Frueholz
Electronics Technology Center, The Aerospace Corporation, Mail Stop: M2-253, P.O. Box 92957, Los Angeles, California 90009
(Received 13 March 1997)

Recent theoretical investigations have shown that when atoms resonantly interact with strong, phase-fluctuating fields of fairly arbitrary character there is an underlying simplicity in their temporal response to the field. Specifically, theory predicts that the atom's response can be divided into two distinct temporal components: an adiabatic component manifesting itself in the instantaneous frame of field-atom interactions as a Bloch-vector trajectory figure-eight pattern, and a nonadiabatic component manifesting itself as population variations oscillating at the Rabi frequency. Here, we experimentally verify theoretical expectations regarding the nonadiabatic component of the field's temporal response. In the presence of a resonant field suffering broadband phase noise we show that atomic population fluctuations display a resonant enhancement at Fourier frequencies corresponding to the Rabi frequency, and that the characteristics of this resonance are similar to those of a damped, driven harmonic oscillator. [S1050-2947(97)09707-2]

PACS number(s): 42.50.Md, 42.50.Ar, 32.80.−t

I. INTRODUCTION

Recently, Frueholz and Camparo [1] theoretically investigated the temporal response of an atomic system to a resonant phase-fluctuating field (PDF) [2]. Though an atom's response to a resonant PDF might appear erratic when viewed in the standard rotating frame of field-atom interactions, Frueholz and Camparo's studies indicate that the erratic appearance belies an underlying simplicity. Briefly, it was found that an atom's temporal response to a resonant PDF is essentially composed of just two components. On time scales long compared to a Rabi period an adiabatic component manifests itself in the instantaneous frame of field-atom interactions as a figure-eight pattern of the Bloch-vector trajectory. Additionally, there is a nonadiabatic component in the atom's temporal response that manifests itself as atomic population variations oscillating at the Rabi frequency Ω, similar to the oscillations of a damped, driven harmonic oscillator with its resonance frequency at Ω. While the adiabatic figure-eight component is only readily apparent in the instantaneous frame, the nonadiabatic component is primarily associated with atomic population variations, and therefore is unchanged by the choice of reference frame (i.e., instantaneous, rotating, or laboratory frame). Consequently, the nonadiabatic component should be easily accessible to experimental investigation, and has relevance to quantum electronic devices such as atomic clocks whose operation depends on atomic population variations.

In general terms, the nonadiabatic variations of a two-level atom's population imbalance, $Z^{\mathrm{nad}}(t)$, can be written as a Fourier series:

$$Z^{\mathrm{nad}}(t)=\sum \zeta_i \sin(2\pi f_i t+\psi_i), \tag{1}$$

where ψ_i is a stochastic phase, f_i is a Fourier frequency, and the ζ_i are Fourier amplitudes. Frueholz and Camparo's key finding regarding $Z^{\mathrm{nad}}(t)$ is that the ζ_i are obtained as solutions to a damped, driven harmonic oscillator:

$$\zeta_i=\zeta(f_i) \cong \frac{Z_0\Omega^2\gamma(\theta_{\mathrm{rms}}^{\mathrm{ad}})^2}{(2\pi f_i)^{n-1}(\gamma^2+\Omega^2)\sqrt{(4\pi^2 f_i^2-\Omega^2)^2+4\pi^2\gamma^2 f_i^2}}. \tag{2}$$

Here, Z_0 is the population imbalance in the absence of the PDF, γ is the atomic relaxation rate, $\theta_{\mathrm{rms}}^{\mathrm{ad}}$ is the rms magnitude of the field's adiabatic phase variations [$\theta(t)$ is the PDF's fluctuating phase], and n is related to the phase variations' power spectral density $S_\theta(f)$ [i.e., $S_\theta(f)\sim f^{-2n}$ with $n\geqslant 1$]. The important point to note from Eqs. (1) and (2) is that the Fourier spectrum of $Z^{\mathrm{nad}}(t)$ exhibits a resonance near $2\pi f_i=\Omega$. Thus, even though the field's phase variations may have a very broad power spectral density, the atom responds preferentially to those Fourier components of the phase variation near the Rabi frequency. Additionally, in the case of strong fields (i.e., $\Omega\gg\gamma$) the amplitude (A) of the resonance has a simple power-law dependence on the Rabi frequency:

$$A\cong\zeta(\Omega)=\frac{Z_0(\theta_{\mathrm{rms}}^{\mathrm{ad}})^2}{\Omega^n}. \tag{3}$$

In the following sections of this paper, we will report on experiments that verify the theoretical predictions embodied in Eq. (2). Specifically, when an atomic system was exposed to a microwave PDF tuned to the atom's ground-state hyperfine transition we observed a resonance in the Fourier spectrum of the atom's population variations, and as predicted by Eq. (2) the resonant frequency was equal to the Rabi frequency. Moreover, the amplitude of the resonance followed the power-law behavior predicted by Eq. (3). Following a description of the experiment in Sec. II, these observations will be described more fully in Sec. III.

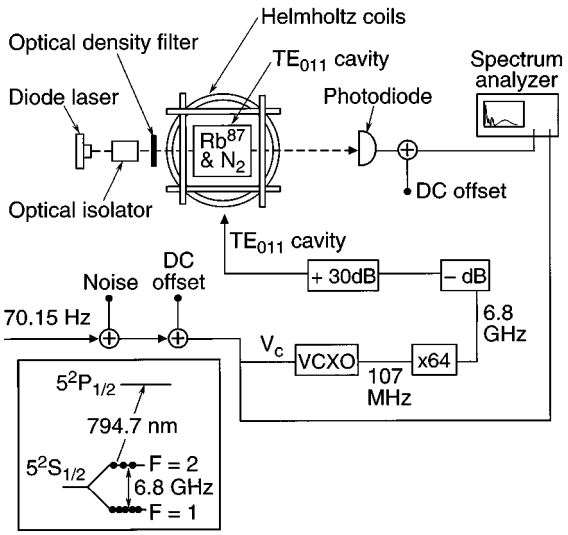

FIG. 1. Optical-pumping–magnetic-resonance experimental arrangement as described in the text. The VCXO had a bandwidth of approximately 10 kHz and a transfer function of -794 Hz/V. The bandwidth of the spectrum analyzer was 25 kHz.

II. EXPERIMENT

The experiment employed an optical-pumping–magnetic-resonance arrangement as illustrated in Fig. 1. A Corning 7070 glass resonance cell containing isotopically pure ^{87}Rb and 10 torr of N_2 was placed in a microwave-cavity whose TE_{011} mode was resonant with the $(F=2,\ m_F=0)$-(1,0) ground state (henceforth, the 0-0) hyperfine transition of ^{87}Rb at 6834.7 MHz. The cylindrical cavity had a radius of 2.8 cm and a length of 5 cm, and the resonance cell filled the cavity volume. Braided windings wrapped around the cavity heated the resonance cell to $\sim 34\,^{\circ}$C, and the entire assembly was centrally located in a set of three perpendicular Helmholtz coil pairs: two pairs zeroed out the Earth's magnetic field while the third pair (~ 300 mG) provided a quantization axis for the atoms parallel to the microwave cavity's cylindrical axis. Light from an $Al_xGa_{1-x}As$ diode laser (~ 3 mW) was tuned to the Rb $5^2P_{1/2}-5^2S_{1/2}(F=2)$ transition [3], and was attenuated by a 2.7 optical density filter before passing through the resonance cell. The transmission of the laser light through the vapor was monitored with a Si photodiode, and the propagation direction of the laser was parallel to the cavity axis.

In the absence of resonant microwaves, optical pumping reduced the density of atoms in the absorbing state [i.e., $5^2S_{1/2}(F=2)$], and consequently increased the amount of light transmitted through the vapor. However, when the microwave field in the cavity was resonant with the ^{87}Rb 0-0 hyperfine transition atoms returned to the $5^2S_{1/2}(F=2)$ state from the $5^2S_{1/2}(F=1)$ state, thereby reducing the amount of transmitted light. Since the alkali vapor was optically thin, the transmitted laser light decreased linearly with the density of atoms in the $F=2$ hyperfine level. The transmitted laser light therefore measured the atomic population's response to the fluctuating microwave field.

The microwaves were derived from a voltage-controlled crystal oscillator (VCXO), which had a modulation bandwidth of 10 kHz [4], and the frequency of its output at ~ 107 MHz was multiplied up into the gigahertz regime before being amplified by a 30-dB solid-state amplifier. The microwave power entering the cavity could be controlled with variable attenuators (labeled as $-$dB in Fig. 1), and these were calibrated to microwave Rabi frequency by measuring the linewidth of the hyperfine transition in the absence of noise [5]. Extrapolating the linewidth measurements to zero microwave power indicated that the intrinsic dephasing rate in our system, γ_2, was approximately 40 Hz. The white noise output from a commercial synthesized function generator was added to a 70.15-Hz sine wave and a dc voltage in order to provide the VCXO's control voltage V_c. The dc level of V_c tuned the average microwave frequency to the 0-0 hyperfine resonance. The sine wave provided adiabatic phase variations, and the noise generator provided stochastic phase fluctuations.

The 70.15-Hz sine wave and noise signal were summed in a preamplifier with an adjustable bandwidth. The low-frequency rolloff of the preamplifier, $\nu_{\rm low}$, at 6 dB/octave was always set at 1 Hz in order to eliminate a dc bias in the noise generator. The high-frequency rolloff, $\nu_{\rm high}$, at 6 dB/octave was typically set at 1 MHz, so that the VCXO was the bandwidth-limiting element in the microwave chain. In our experiments, Ω was always less than 10 kHz. Thus, with $\nu_{\rm high}=1$ MHz we always had $S_\theta(f\cong\Omega/2\pi)\sim f^{-2}$ (i.e., $n\cong 1$) [6]. In one set of experiments, though, $\nu_{\rm high}$ was set equal to 550 Hz. In this latter experiment, when Ω was greater than 550 Hz, we had $S_\theta(f\cong\Omega/2\pi)\sim f^{-4}$ (i.e., $n\cong 2$). The amplitude of the sine wave and the amplitude of the noise voltage could be adjusted in order to vary $\theta_{\rm rms}^{\rm ad}$ and the standard deviation of the phase variations, respectively. (Since phase variations and microwave frequency variations are related, for ease of discussion we will refer to the microwave signal's deterministic and stochastic variations in terms of the amplitude of sinusoidal frequency variations, $\delta\omega_{\rm sine}$, and the standard deviation of microwave frequency fluctuations, σ_ω, respectively in what follows.)

III. RESULTS

A. Resonance behavior

Figure 2(a) shows the power spectrum of the VCXO control voltage. As expected the power spectrum is composed of a bright line at 70.15 Hz, corresponding to the adiabatic phase variations, and a constant background corresponding to the stochastic phase fluctuations. Figure 2(b) shows the power spectrum of the transmitted light intensity $S_I(f)$ for several different values of the Rabi frequency. Specifically, Fig. 2(b) corresponds to $\Delta S_I(f)\equiv[S_I^{\rm noise}(f)-S_I^{\rm no\ noise}(f)]$. For these experiments $\sigma_\omega=\pm 490$ Hz, $\nu_{\rm high}=1$ MHz, and $\delta\omega_{\rm sine}=2.5$ kHz. Clearly, the atom's response to the field shows a resonant behavior that is not present in V_c, and as predicted by Eq. (2) the resonance's center frequency and amplitude are functions of the Rabi frequency. This latter dependence is better illustrated in Fig. 3, where the center frequency [Fig. 3(a)] and the amplitude [Fig. 3(b)] of the resonance are plotted as a function of Rabi frequency. The dashed line in Fig. 3(a) has a slope of 1.0, indicating equality between the resonance frequency and the Rabi frequency as measured by the linewidth of the 0-0 hyperfine

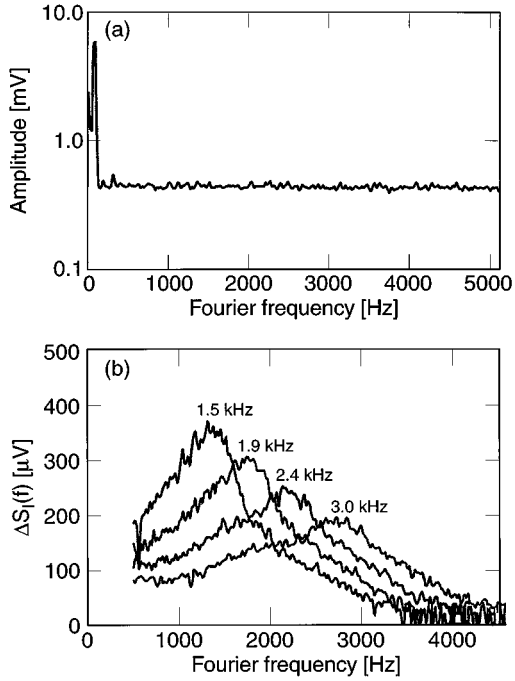

FIG. 2. (a) Fourier spectrum of the VCXO control voltage V_c when V_c included both sinusoidal and stochastic variations. (The spectrum analyzer resolution was 30 Hz, and with $V_c=0$ the Fourier spectrum was flat with an amplitude of a 4 μV.) Note that the spectrum of V_c is flat except for the bright line at 70 Hz corresponding to the sine wave phase modulation. (b) Fourier spectrum of the transmitted light intensity in the presence of broadband phase noise [i.e., $\Delta S_1(f)$] with $\delta\omega_{\text{sine}}=2.5$ kHz, $\sigma_\omega=\pm 490$ Hz, and $\nu_{\text{high}}=1$ MHz. The various curves are labeled by the Rabi frequency employed in the experiment, and again the spectrum analyzer resolution was 30 Hz.

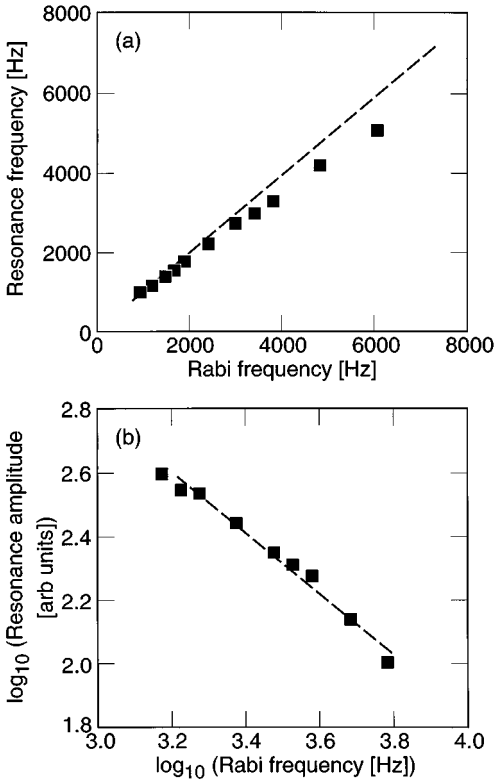

FIG. 3. (a) Resonance frequency as a function of Rabi frequency for the experimental parameters of Fig. 2. The dashed line corresponds to equality between the resonance frequency and the Rabi frequency as measured by the linewidth of the observed 0-0 hyperfine transition. (b) Resonance amplitude as a function of Rabi frequency for the same parameters as Fig. 2. The dashed line is a linear least-squares fit to the data and has a slope of -0.96.

transition. The dashed line in Fig. 3(b) corresponds to a linear least-squares fit to the data on the log-log plot and results in a slope of -0.96. This last result is consistent with the predictions of Eq. (3), since as discussed in Sec. II we expect $n\cong 1$ for $\nu_{\text{high}}=1$ MHz.

Given the mode structure of the microwave field within the cavity, and the relative immobility of the Rb atoms [7], atoms in different regions of the vapor experience different Rabi frequencies. The observed signal is therefore a weighted sum of contributions from the various regions, so that the observed temporal response of the alkali vapor corresponds to an averaged Rabi frequency. For the same reason, the power-broadened linewidth of the 0-0 hyperfine resonance also corresponds to an averaged Rabi frequency [8]. Though the average Rabi frequency derived from the measured linewidth and the average Rabi frequency derived from the atom's temporal behavior should be approximately equal, there is no reason to expect the two average values to be exactly the same; generation of the two signals may weigh the contributions of various regions within the cavity slightly differently. Thus, it is not surprising that the data of Fig. 3(a) do not fall exactly on the dashed line. Clearly, though, the near equality between the average Rabi frequency as measured by the 0-0 linewidth and the resonance frequency validates Eq. (2).

B. Dependence of the resonance amplitude on Rabi frequency

Though the data of Fig. 3(b) are consistent with Eq. (3), the data do not completely validate Eq. (3). Equation (3) indicates that the power-law relationship between the resonance amplitude and the Rabi frequency is determined by the power-law relationship between the phase's spectral density and Fourier frequency in the vicinity of the Rabi frequency [i.e., the value of n appearing in Eq. (3) comes from $S_\theta(f\cong\Omega/2\pi)$]. Therefore, to validate Eq. (3) one should clearly demonstrate that $S_\theta(f\cong\Omega/2\pi)\sim f^{-2n}$ implies $\zeta(\Omega)\sim\Omega^{-n}$. To this end, we remeasured the amplitude of the resonance as a function of Ω with $\nu_{\text{high}}=550$ Hz. For this value of the high-frequency rolloff,

$$\Omega>550 \text{ Hz}\Rightarrow S_\theta(f\cong\Omega/2\pi)\sim f^{-4}\Rightarrow n=2,$$

while

$$\Omega<550 \text{ Hz}\Rightarrow S_\theta(f\cong\Omega/2\pi)\sim f^{-2}\Rightarrow n=1.$$

The results from the experiment are shown in Fig. 4, where resonance amplitude is plotted as a function of Rabi frequency. To obtain the data of Fig. 4(a), parameters were chosen that optimized the resonance in the regime of high Rabi frequencies, $\Omega>550$ Hz, (i.e., $\delta\omega_{\text{sine}}=1.5$ kHz and $\sigma_\omega=\pm 244$ Hz). The straight line in Fig. 4(a) is a least-squares fit to the log-log data, and has a slope of -2.0. To

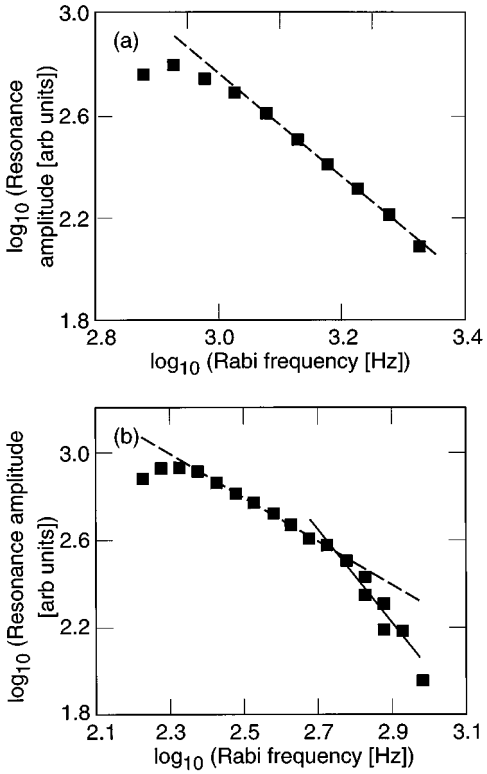

FIG. 4. Resonance amplitude as a function of Rabi frequency for $\nu_{\text{high}}=550$ Hz. (a) To optimize the resonance $\delta\omega_{\text{sine}}=1.5$ kHz, $\sigma_\omega=\pm 244$ Hz. The dashed line is a least-squares fit to the data with a slope of -2.0. (b) To optimize the resonance $\delta\omega_{\text{sine}}=508$ Hz, $\sigma_\omega=\pm 41$ Hz. The dashed line is a least-squares fit to the lower Rabi frequency data with a slope of -1.0, and the solid line is a least-squares fit to the higher Rabi frequency data with a slope of -2.2.

obtain the data of Fig. 4(b), parameters were chosen that optimized the resonance in the regime of low Rabi frequencies, $\Omega\approx 550$ Hz, (i.e., $\delta\omega_{\text{sine}}=508$ Hz and $\sigma_\omega=\pm 41$ Hz). The dashed line in Fig. 4(b) is a least-squares fit to the low Rabi frequency data, $\Omega<\nu_{\text{high}}$, and this has a slope of -1.0. The solid line in Fig. 4(b) is a least-squares fit to the higher Rabi frequency data, $\Omega>\nu_{\text{high}}$, and this has a slope of -2.2. The fact that the resonance amplitude has a power-law dependence on Ω, and that the exponent of the power-law dependence is determined by $S_\theta(f\cong\Omega/2\pi)$ provides strong evidence of the validity of Eq. (3).

C. Dependence of resonance amplitude on adiabatic phase variations

A further prediction of Eq. (2) is that the amplitude of the resonance is proportional to $\theta_{\text{rms}}^{\text{ad}}$. For a fixed adiabatic modulation frequency this is equivalent to a proportionality between the resonance amplitude and $\delta\omega_{\text{sine}}$. In the experiment to test this prediction the Rabi frequency and phase noise were held constant, and the amplitude of the resonance was measured as a function of $\delta\omega_{\text{sine}}$. The results are shown in Fig. 5, and the linear relationship between the resonance amplitude and $\delta\omega_{\text{sine}}$ provides further evidence for the validity of the theory presented in Ref. [1] (see Ref. [9]).

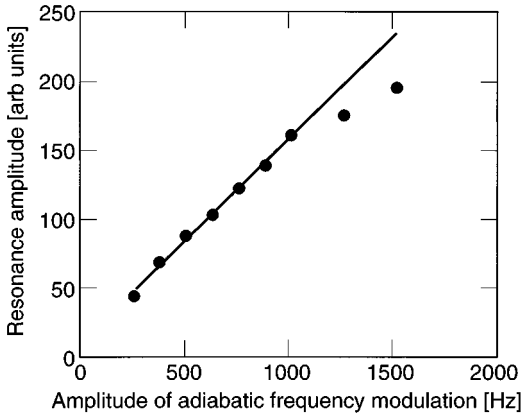

FIG. 5. Resonance amplitude as a function of the amplitude of the sinusoidal, adiabatic frequency modulation for $\Omega=2.4$ kHz, $\sigma_\omega=\pm 490$ Hz, and $\nu_{\text{high}}=1$ MHz. The solid line is a linear least-squares fit to the data. Deviation from the linear relationship at large values of $\delta\omega_{\text{sine}}$ is most likely due to a breakdown of first-order perturbation theory for these frequency modulation amplitudes.

IV. SUMMARY

We have experimentally verified certain theoretical predictions made in Ref. [1] regarding an atom's response to a PDF. Generally, we found that the atom's response was similar to that of a damped, driven harmonic oscillator. More specifically, we found that (1) the Fourier spectrum of the atom's population fluctuations showed a resonance at the Rabi frequency, (2) the amplitude of this resonance obeyed a power-law relationship with the Rabi frequency, (3) the exponent of the power-law relationship was determined by the spectral density of field phase fluctuations, and (4) the amplitude of the resonance depended on the magnitude of adiabatic phase variations.

Though an atom's temporal response to a phase fluctuating field might appear erratic, the present work in combination with Ref. [1] demonstrates that in the regime of strong fields (i.e., saturation) this erratic behavior belies an underlying simplicity. In particular, though it is well known that a PDF induces population fluctuations in a resonant atomic system [10], the present work demonstrates that the dominant Fourier components associated with the atomic fluctuations cluster around the Rabi frequency. This observation has relevance to various quantum electronic devices such as atomic clocks, where phase modulation of a resonant field induces atomic population modulation, which in turn generates the device's signal. The present work suggests that noise associated with phase modulation in such devices will give rise to noise in the device's signal at Fourier frequencies near the atomic system's Rabi frequency. In future work we intend to show that the underlying simplicity in an atom's response to a PDF is maintained even for nonresonant PDFs.

ACKNOWLEDGMENTS

The authors would like to thank B. Jaduszliwer for several stimulating discussions regarding the experimental findings, and a critical reading of the manuscript. This work was supported under Air Force Contract No. FO4701-93-C-0094.

[1] R. P. Frueholz and J. C. Camparo, Phys. Rev. A **54**, 3499 (1996).

[2] Rigorously, the term PDF (i.e., phase-diffusion field) should be reserved for fields whose phase variations undergo a random walk. However, for ease of discussion we are generalizing the acronym in this paper so as to refer to any field whose phase fluctuations have a non-white power spectral density.

[3] J. C. Camparo, Contemp. Phys. **26**, 443 (1985); C. E. Wieman and L. Hollberg, Rev. Sci. Instrum. **62**, 1 (1991).

[4] A VCXO has an output frequency that is approximately proportional to a control voltage V_c. For a brief discussion of VCXO characteristics see R. L. Kent, in *Proceedings of the 19th Annual Symposium on Frequency Control, Atlantic City, NJ, 1965* (National Technical Information Service, Springfield, VA, 1965), pp. 642–654.

[5] J. C. Camparo and R. P. Frueholz, Phys. Rev. A **31**, 1440 (1985); and J. C. Camparo and R. P. Frueholz, *ibid.* **32**, 1888 (1985).

[6] Defining $S_\omega(f)$ as the spectral density of microwave frequency fluctuations and $S_\theta(f)$ as the spectral density of microwave phase variations, $S_\omega(f)=4\pi^2 f^2 S_\theta(f)$; see L. S. Cutler and C. L. Searle, Proc. IEEE **54**, 136 (1966). Thus, for $S_\omega(f)=\text{const}$, $S_\theta(f)\sim f^{-2}$.

[7] R. P. Frueholz and J. C. Camparo, J. Appl. Phys. **57**, 704 (1985).

[8] J. C. Camparo and R. P. Frueholz, Phys. Rev. A **30**, 803 (1984); J. C. Camparo, *ibid.* **39**, 69 (1989).

[9] At large values of the sinewave voltage we found that the amplitude of the resonance saturated. This, however, is not at odds with the predictions of Eq. (2), as the analysis of Ref. [1] employs a first-order perturbation theory. For microwave frequency modulation amplitudes greater than the Rabi frequency, it is to be expected that the predictions of Eq. (2) would break down.

[10] See, for example, A. A. Rangwala, K. Wodkiewicz, and C. Su, Phys. Rev. A **42**, 6651 (1990); M. H. Anderson, R. D. Jones, J. Cooper, S. J. Smith, D. S. Elliot, H. Ritsch, and P. Zoller, *ibid.* **42**, 6690 (1990), and references therein.